Giant magnetoresistance in the crystalline YCd_6 intermetallic compound

M. Cabrera-Baez,[1] K. V. R. A. Silva,[1] P. R. T. Ribeiro,[1] D. R. Ratkovski,[1] E. L. T. França,[1] A. Flessa-Savvidou,[2,3] B. Casas,[2] T. Siegrist,[2,4] L. Balicas,[2,3] S. M. Rezende,[1] and F. L. A. Machado[1,2,*]

[1]*Departamento de Física, Universidade Federal de Pernambuco, 50670-901, Recife, PE, Brazil*
[2]*National High Magnetic Field Laboratory, Tallahassee, Florida 32310, USA*
[3]*Department of Physics, Florida State University, Tallahassee, Florida 32306, USA*
[4]*FAMU-FSU College of Engineering, Tallahassee, Florida 32310, USA*

(Received 5 December 2022; revised 15 February 2023; accepted 24 March 2023; published 10 April 2023)

Giant magnetoresistance (GMR) in bulk nonmagnetic compounds has received considerable attention since this phenomenon challenged the classical understanding of electron transport under a magnetic field. Here, we report magnetotransport properties of the diamagnetic intermetallic compound YCd_6 for applied magnetic fields up to 35 T and temperatures down to 0.4 K that reveal GMR. We argue that the large MR value can be explained in terms of field-induced pseudogaps on a Fermi surface. These results are relevant to the understanding of the Fermi-surface topology of quasicrystal approximants.

DOI: 10.1103/PhysRevB.107.144414

I. INTRODUCTION

Since the discovery of giant magnetoresistance (GMR) in multilayers of Fe/Cr, magnetoresistance (MR) has become one of the most studied properties of materials due to its implications in sensor devices, magnetic memory, and read head technology. Although GMR was observed in artificial multilayers [1], naturally layered compounds are an important alternative for understanding the fundamental issues concerning transport in two- and three-dimensional (2D and 3D) materials [2]. GMR has been observed in naturally layered magnetic and nonmagnetic systems. In the first case, investigations in rare-earth-based intermetallic systems have been attracting the attention of researchers for several decades [3,4] since the resistivity can become complex in view of the coexistence between localized and itinerant spins. The resistivity can have two major contributions from the conduction electron relaxation time and density. Recently, topological semimetals renewed the interest in this class of systems because they host intriguing magnetic and electric properties [5]. Large magnetoresistance in single-crystal semimetals such as $(W, Mo)Te_2$, $(Nb, Ta)Sb_2$, Cd_3As_2, etc., has been revealed ranging from $10^5\%$ to $10^6\%$ at magnetic field around 9 T and $T \sim 2$ K [5–8]. In addition, MR was also detected in nonmagnetic metallic systems such as $PdCoO_2$ [9] and $PtSn_4$ [10] with high carrier density reaching $10^4\%$–$10^5\%$ at 14 T and 2 K.

The physical explanation of MR in semimetals relies on models involving two bands resulting in large parabolic field-dependent MR [11]. In the case of metals as $PtSn_4$, these large magnetic field effects on transport properties are mainly due to different mobility changes for the different types of carriers. The anisotropic field response on MR in $PtSn_4$ indicates a complicated electronic structure [10]. In the same line of nonmagnetic metallic systems, the case of the cubic intermetallic system YCd_6 is relevant due to the connection with the icosahedral quasicrystal i-Y-Cd [12,13]. RCd_6 (R: rare earth) compounds are known as quasicrystal approximants (QCAs) to the icosahedral quasicrystals (QCs) i-R-Cd [14] where some of the QCs have a long-range orientational order but lack a periodic translational order.

Up to now, no MR studies have been reported in members of the family of RCd_6 because it is uncommon in nonlayered systems. Particularly, the QCA YCd_6 has a body-centered-cubic (bcc) crystal structure (space group $Im\bar{3}$) composed of the so-called Tsai-type icosahedral cluster, as shown in Fig. 1. YCd_6 is an intermetallic crystalline compound with a complex unit cell characterized by a strong diamagnetic behavior almost independent of the temperature from dc magnetic susceptibility measurements [14]. This metallic system exhibits a small Sommerfeld coefficient of 9(4) mJ/mol K^2 giving 1.3 mJ/mol K^2 per atom compatible with elemental metals such as Cu, Al, etc. [14]. These results point out YCd_6 as an uncorrelated simple system.

Recently, in a microscopic point of view, electron spin resonance (ESR) experiments on Gd^{3+}-doped single crystals of YCd_6 reveal the existence of various electronic bands at the Fermi level where a different degree of electronic localization was measured [15]. More itinerant electrons called s type were responsible for the observed exchange bottleneck phenomena and the relaxation of the magnetic probe was also with p-type and d-type conduction electrons. The combination of the already reported density functional theory (DFT) calculations on YCd_6 [16] and the experimental study using ESR supports unequivocally a multiband scenario of this compound and future explorations on transport properties may take this as a starting point. Here, we report GMR at low temperatures and high applied magnetic fields in YCd_6 showing striking dependencies with the applied magnetic field.

*Corresponding author: fernando.machado@ufpe.br

 ©2023 American Physical Society

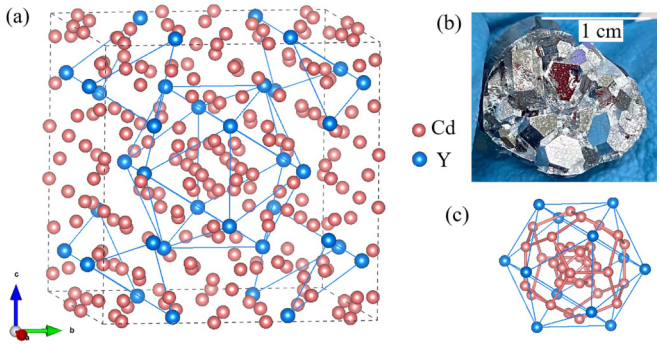

FIG. 1. (a) Crystal structure of the cubic YCd_6 intermetallic system. (b) Typical polyhedral samples. (c) Cages formed by Y and Cd atoms.

II. EXPERIMENTS

A. Sample preparation and characterization

A batch of YCd_6 single crystals was grown by the standard self-flux method [17] using an excess of Cd following the available phase diagram [12]. The constituent elements were 99.9% Y and 99.999% Cd (Alfa-Aesar). The initial ratios of elements were 7:93 for Y:Cd based on previously reported growths [15]. The elemental mixtures were sealed in an evacuated quartz ampoule and placed in a box furnace for the subsequent increase in temperature. Crystals were grown by slowly cooling the melt between 700 and 500 °C over 100 h. At 500 °C the ampoules were removed from the furnace, inverted, and placed in a centrifuge to spin off the Cd excess flux. The separated crystals are typically polyhedral of ∼4 mm or larger [Fig. 1(b)].

X-ray diffraction (XRD) of polycrystalline YCd_6 was performed by using a Rigaku Smartlab diffractometer. Crystalline pieces of YCd_6 were transformed into a powder sample using an agate mortar. Figure 2 shows an x-ray diffractogram obtained at room temperature collected in the angular range $20° \leqslant 2\theta \leqslant 85°$ measured in steps of 0.01° and with an acquisition time of 1 s per step. The XRD data indicate that the obtained samples are single phase and display the previously reported crystalline structure [18]. The position of the peaks corresponds to the ones expected for a cubic phase according to the ICSD-191849 [19]. Energy dispersive spectroscopy (EDS) was also used to characterize the sample yielding the composition in weight percent (wt %) with values that are very close to the nominal composition: $Y_{12.9}Cd_{86.4}$. A rather small peak of about 0.7 wt % of Al from the sample holder was also observed. The EDS spectrum is shown in the upper inset in Fig. 2. The mass density (ρ_m) was measured in a gas pycnometer model Accupyc II 1340 made by Micromeritics at $T = 298$ K. A sample with mass of 1228.6 ± 0.1 mg was placed in a 10 cm^3 crucible filled with a helium gas atmosphere at a pressure 1.34×10^{-5} Pa yielding $\rho_m = 7.65 \pm 0.13$ g/cm^3.

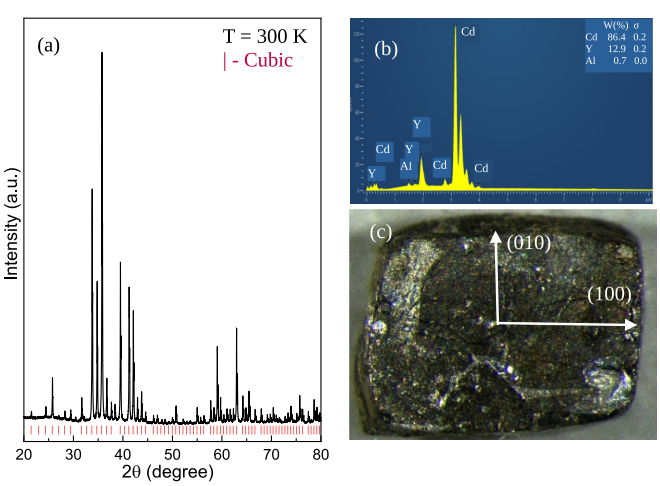

FIG. 2. (a) Room-temperature x-ray diffraction data for a polycrystalline sample of YCd_6. (b) EDS spectrum and (c) a photograph indicating the (010) and (100) directions of the measured single crystal.

MR measurements for the temperature range $2\ \text{K} \leqslant T \leqslant 300$ K and $\mu_0 H$ under magnetic fields up to $\mu_0 H = 8.5$ T were performed using the resistivity option of a Quantum Design physical properties measurement system (PPMS). The four leads between the sample and the PPMS puck were attached with silver paint. The dc electrical current used in these measurements was 5 mA. The PPMS ac measurements modulus was employed for measuring the T dependence of the ac magnetic susceptibility (χ_{ac}) in the same range of T's by keeping the magnitude of the ac magnetic field constant ($h_{ac} = 10$ Oe) and by varying the frequency (f) from $f = 30$ to 10^4 Hz.

The MR was also measured at temperatures as low as $T = 0.4$ K under magnetic fields up to 35 T using a four-probe technique. These measurements were performed using a dc magnet equipped with a liquid ^{3}He cryostat in Cell 12 at the National High Magnetic Field Laboratory at Tallahassee. A calibrated Cernox thermometer connected to a LakeShore ac resistance bridge model 370 was used for measuring the ^{3}He bath temperature. The YCd_6 sample was mounted on a rotating sample holder that allowed to vary the direction of the applied magnetic field relative to the electrical current from a parallel to a perpendicular configuration. The crystallographic orientations were determined via Laue x-ray diffraction, as depicted in Fig. 2(c), using the well-defined faces of the single-crystal cut in those same directions using a diamond wire saw. The electrical contacts were also made with silver paint. A Keithley current source model 6221 was used to inject an ac electrical current through the sample along the (100) direction. The magnitude and frequency of the ac electrical current used to measure the MR were, respectively, 1.0 mA and 13.77 Hz and the voltage across the sample was measured using a Stanford Research Systems lock-in amplifier model SR860. The electrical resistance data were recorded while the magnetic field was continuously ramped with a sweep rate of 2 T/min.

B. Experimental results

Figure 3(a) shows the measured metalliclike T dependence of the in-plane resistivity (ρ) of YCd_6 under a perpendicular magnetic field with field strengths $\mu_0 H = 0$ T (dark blue spheres) and 8.5 T (red circles). At room temperature, the zero-field resistivity $\rho(\mu_0 H = 0)$ is 10.8 $\mu\Omega$ cm and de-

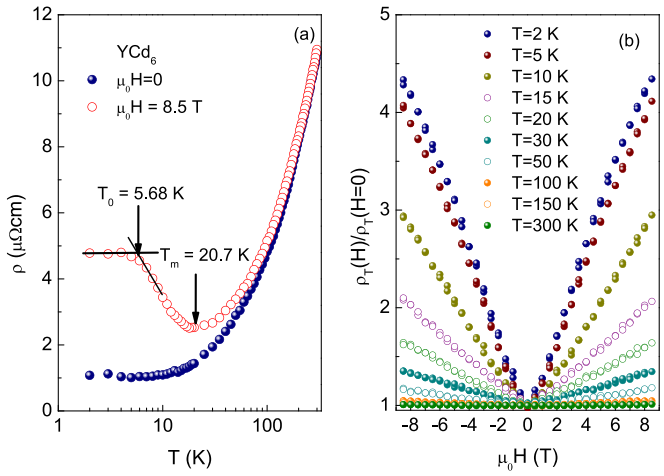

FIG. 3. (a) Resistivity vs T measured in the range 2–300 K for $\mu_0 H = 0$ and 8.5 T. Note that the resistivity becomes nearly T independent below 5.68 K. (b) Relative resistivity vs field strength H for several values of T.

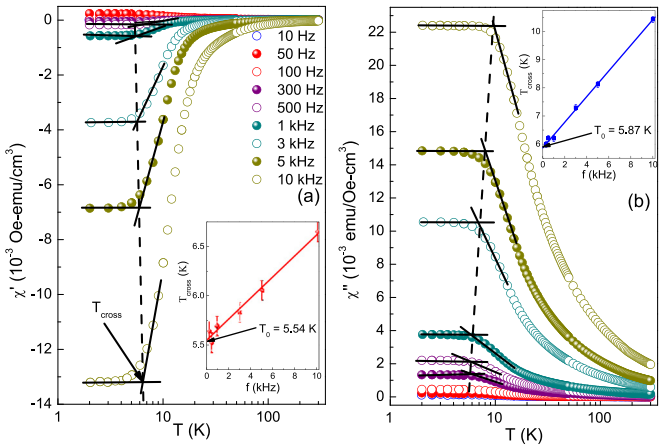

FIG. 4. Temperature dependence of the (a) in-phase and (b) out-of-phase components of the ac magnetic susceptibility for the frequencies f indicated.

creases monotonically with decreasing T down to 1.2 $\mu\Omega$ cm yielding a residual resistivity ratio RRR = 9. This value is slightly higher than the previously reported value for YCd_6 single crystals [14] and may be related to the purity of the elemental Y. For $\rho(\mu_0 H = 8.5)$ T it is possible to observe a similar metallic behavior above 110 K when compared with $\rho(\mu_0 H = 0)$. As the temperature decreases, strong differences appear below 100 K where the resistivity decreases from 100 K to $T_m = 20.7$ K and then increases abruptly until $T_0 = 5.68$ K is reached, followed by saturation below T_0. T_m corresponds to the temperature at which the slope of the resistivity as a function of T changes from positive to negative. T_0 is the temperature where the resistivity begins to saturate at low T's.

Figure 3(b) shows the MR as a function of $\mu_0 H$ measured at several temperatures revealing remarkable features. First, the resistivity has a relatively weak field dependence above 50 K but depends strongly on magnetic field below this temperature. Second, there is no evidence for saturation of the MR signal in the explored range of temperatures and fields. The magnetic field dependences of the MR curves are paraboliclike at high temperatures (above 50 K) but display a clear evolution towards linear behavior below 50 K.

Figure 4 shows the temperature dependence of the in-phase, χ' [Fig. 4(a)], and out-of-phase, χ'' [Fig. 4(b)], components of the ac magnetic susceptibility for $f = 30$, 50, 100, 300, 500, 1000, 3000, 5000, and 10 000 Hz and $\mu_0 H_{ac} =$ 1 mT applied along the (100) direction. Note that both components become nearly T independent below some f-dependent value as indicated by T_{cross} (see Fig. 4). The insets in both figures show the linear dependence of T_{cross} yielding similar values of $T_0 \sim 5.54$ K in Fig. 4(a) and $T_0 \sim 5.87$ K in Fig. 4(b) at $f = 0$ and also compatible with $T_0 \sim 5.68$ K from Fig. 3(a). It is worth noting the clear evolution of χ' (from $\sim$0 to -13×10^{-3} Oe emu/cm^3) and χ'' (from $\sim$0 to 23×10^{-3} emu/Oe cm^3) at $T = 2$ K for different frequencies.

As shown in Fig. 3(b), the field dependence of the MR changes between high and low temperatures. To better understand these features and complement the above information, we studied the MR under high magnetic fields.

Figure 5(a) presents $\rho(\mu_0 H)$ for magnetic fields up to $(\mu_0 H) = 35$ T (perpendicular to the electrical current) and temperatures from $T = 25.0$ to 0.42 K where it is possible to infer a continuous evolution on its field dependence, i.e., from linear (unsaturated) behavior ($T \sim 25$ K) to a saturated response of $\rho(\mu_0 H)$ at $T \sim 0.4$ K. The data for $T = 0.42$ and 25 K are shown for both positive and negative values of H while for the other values of T they are shown for positive values of H only. The inset is a zoom in of the central part of the magnetoresistance data revealing that below about 50 mT the MR approaches zero in a somewhat faster magnetic field dependence, perhaps associated to a possible superconductivity transition in YCd_6 and/or little residual Cd flux at the surface (EDS at various locations ensures internal homogeneity of the YCd_6 sample). This low-T superconducting behavior (below 1.8 K) is not relevant and does not interfere with the MR analysis. As expected, the observed linear dependence is consistent with the data presented in Fig. 3(b).

To better understand the evolution of the resistivity as a function of the magnetic field, Fig. 5(b) shows $\rho(\mu_0 H)$ for values of $\mu_0 H$ up to 35 T and the corresponding fit to a power law (black line) for four values of T. The inset shows the exponent of the field dependence $\rho(\mu_0 H) = \alpha(T)(\mu_0 H)^\eta$ featuring a linear and continuous evolution from $\eta = 1$ to 0.5 above $T_0 = 5.65$ K followed by saturation below T_0. A remarkable result is the T_0 value that is in perfect agreement with the data presented in Figs. 3 and 4 as indicated above.

The single-crystalline anisotropic properties of $\rho(\mu_0 H)$ were also explored by varying the orientation of the applied magnetic field. Figure 6(a) presents ρ as a function of $\mu_0 H$ data for several values of T with $\mu_0 H$ applied parallel to the electrical current. The data for $T = 0.42$ and 25 K are shown for both positive and negative values of $\mu_0 H$ while for the other values of T the data are displayed for positive values of $\mu_0 H$ only. The inset shows the exponent of the power law obtained for all values of T yielding values of η between 0.7 and 0.3. Figure 6(b) shows ρ vs $\mu_0 H$ for several values of the angle between $\mu_0 H$ and the electrical current. The inset shows

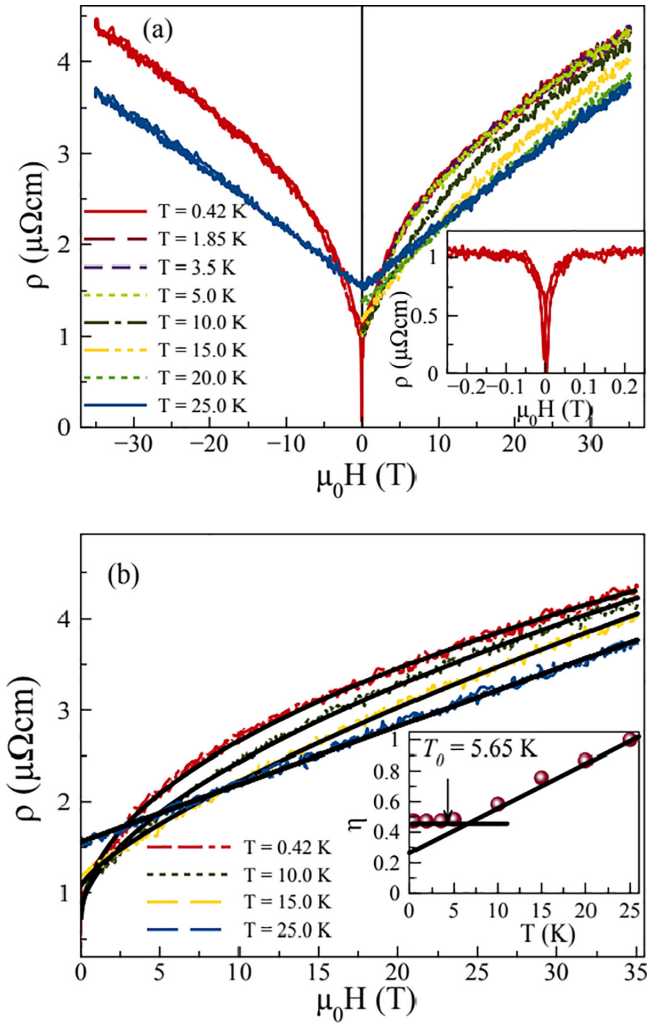

FIG. 5. (a) Low-T ρ vs H data for several values of T with H applied perpendicular to the electrical current. The data for $T = 0.42$ and 25 K are shown for both positive and negative values of H while for the other values of T are for positive values of H only. The inset is a blowup of the central part of the magnetoresistance data. (b) ρ vs H data and the corresponding fit to a power law (black line) for four values of T. The inset shows the exponent of the power law obtained for all values of T.

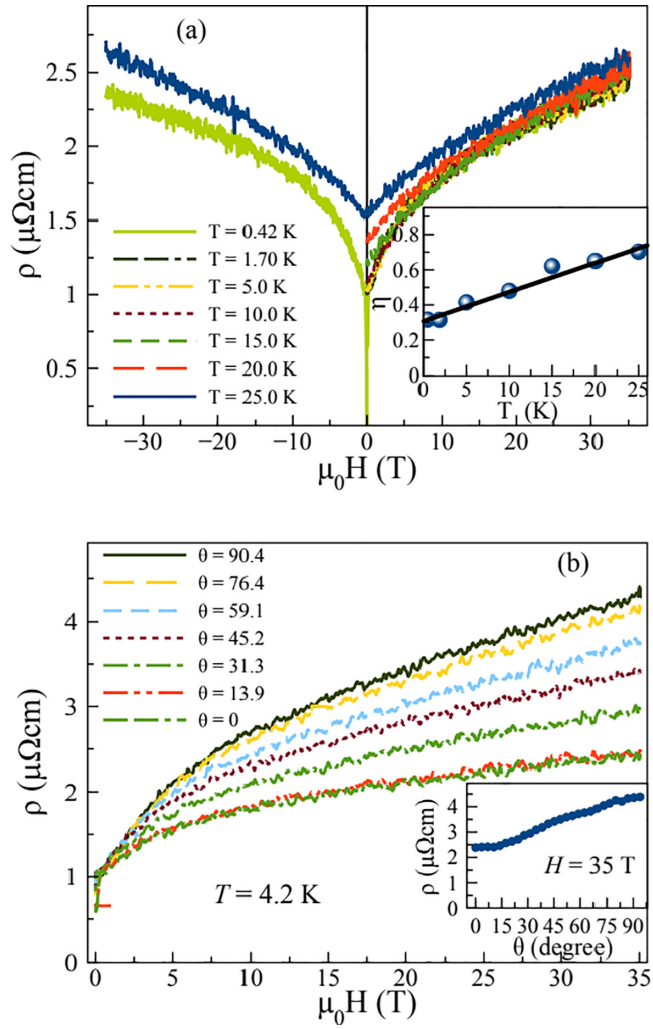

FIG. 6. (a) Low-T ρ vs $\mu_0 H$ data for several values of T with $\mu_0 H$ applied parallel to the electrical current. The inset shows the exponent of the power law obtained for all values of T. (b) Low-T ρ vs $\mu_0 H$ for several values of the angle between $\mu_0 H$ and the electrical current. The inset shows the magnitude or the resistance for $\mu_0 H = 35$ T obtained from a larger set of ρ-$\mu_0 H$ data.

the magnitude of the resistance for $\mu_0 H = 35$ T obtained from a larger set of ρ-$\mu_0 H$ data. Notice that the data for $\mu_0 H$ parallel to the electrical current are significantly smaller than the data measured with $\mu_0 H$ perpendicular to I, as expected.

III. ANALYSIS AND DISCUSSION

The MR of many metals and semimetals can be represented by the form $\Delta\rho/\rho(0) = G[H/\rho(0)]$ commonly referred to as Kohler's rule, where $G(H)$ usually follows a power law, depending on the geometrical configurations and on the materials [20]. In a simple case of a metal, one may find the relation $\rho/\rho(0) \sim (\omega_c \tau)^2$, where $\omega_c = eH/m_e$ is the cyclotron frequency [21]. The observed behavior of $\rho/\rho(0) \sim H^2$ (orbital motion of conduction electrons) is close to what is expected for an ordinary metallic compound with no open orbits [22]. For instance, this relation is satisfied by the $PtSn_4$ compound [10] (which exhibits a very large transverse magnetoresistance of $\sim 10^5$%) although its behavior differs markedly from the low T results obtained for YCd_6. As shown in Figs. 3 and 5, the field dependence of the MR of YCd_6 evolves from $\rho/\rho(0) \sim (\mu_0 H)^2$ above 50 K to $\sim(\mu_0 H)^1$ (25 K $\leqslant T \leqslant$ 50 K), and to $\sim H^{0.5}$ upon further cooling (0.4 K $\leqslant T \leqslant$ 5.65 K) in transverse MR experiments (TMR). In the case of longitudinal MR (LMR), a continuous evolution of exponent on $\mu_0 H$, i.e., from 0.8 to 0.3, was observed (see Fig. 6 inset).

Although the MR is not simply related to the topology of the Fermi surface (FS), the TMR and LMR data measured for YCd_6 at low temperatures and high magnetic fields (Figs. 3, 5, and 6) indicate anisotropy in the band structure. For YCd_6, different densities of charge carriers with different mobilities that would depend on the temperature may contribute to the field dependence of ρ, leading to the super- or sublinear

trends. Similar behavior was observed in $PdCoO_2$ and $PtCoO_2$ nonmagnetic metallic systems [9,23]. For these systems, the $MR(H) \sim H^{0.5}$ dependence is related to the existence of more than one length scale around the FS [23,24]. Particularly, for the case of $PdCoO_2$, Varnavides *et al.* proposed diffusive, ballistic, and hydrodynamic transport regime limits [25]. To compare with our data, some interesting results evidence TMR in metals at high fields as was the case of Li, Zn, Pt, Ag, Sn, Au, Ni, and Pb [26] where MR of Pb followed a $H^{0.5}$ dependence. It turns out that having two types of carriers with different mobilities can lead to sublinear MR when one is approaching its saturation. To explain the $H^{0.5}$ and H^1 behavior, the authors suggest the contact between the Brillouin-zone face and the FS. Although relevant, these experiments were carried out using polycrystals where an average over all microcrystalline directions may contribute to the magnetic field dependence of MR. The case of YCd_6 shows a complete differentiation depending of the orientation of the magnetic field because we use single-crystalline samples.

For LMR results, one does not expect the motion of electrons along the field to be affected but this is only true to free electrons but not to electrons in metals [27]. Evidently, Fig. 6 shows nonzero LMR results as expected in real metals showing a saturation trend for high fields with T-dependent exponents. Similar results were observed in elemental metals such as Ag and Cu where the existence of necks on the FS and two types of scattering mechanisms were postulated [27]. When and electron passes through a neck, it suffers Bragg reflection and its velocity is almost exactly reversed where, at high magnetic fields, the current carried by the electrons with orbits through a neck is very reduced [27]. It is worth mentioning that the FS topology of Ag and Cu is far away to be comparable with the case of YCd_6 for obvious reasons but, in a similar way, an LMR effect can result from FS anisotropy [20,28,29].

With this, a possible explanation of the anisotropic H dependence of MR may be related to the existence of different electron bands at the FS. Previous DFT calculations on YCd_6 confirm the presence of s-, p-, and d-type conduction electrons and report a small midgap peak just above the Fermi level [16]. In a Fermi-liquid scenario, conduction electrons with different effective masses (delocalized in energy bands) could follow different cyclotron orbits in a magnetic field. In this multiband system, it is reasonable to assume more extended orbits for s-type conduction electrons when compared to p and d (assuming different localization degrees). Without magnetic field, the conductivity is dominated by s, p, and d carrier types. But with magnetic field, then it is possible that only s-type electrons conduct. This assumption is in agreement with the observed magnetoresistive effect in Fig. 3(a). A different degree of localization of conduction electrons is a well accepted concept in view of the complex FS. Previous ESR experiments in this system support this possible scenario [15] although a detailed investigation of the Fermi surface of YCd_6 (experimental or theoretical) could provide better clues about a satisfactory explanation.

Other interesting system evidencing large magnetoresistance is the case of $MoTe_2$ [6] which is a noncompensated semimetal where the number of hole carriers is higher than electron carriers. This system shows nonsaturating extremely large magnetoresistance attributed to a combination of Fermi-surface deformation and spin orbit interactions in the presence of external magnetic field. Similar results were observed in $NbSb_2$ [30] with strong MR anisotropy where MR is attributed to the change of the Fermi surface (Dirac-like point) induced by the magnetic field. The mechanism responsible for the observed MR is related to the creation of a gap in the two Dirac-like points induced by the external magnetic field. These observations imply the inadequacy of the FS compensation picture in $NbSb_2$ [30] in contrast with the $PtSn_4$ scenario. The case of $PtSn_4$ exhibits a minimum on the temperature dependence of the resistivity in a magnetic field due to the transition from high effective magnetic fields to weak ones [31]. This is observed in compensated conductors with a closed FS. The case of YCd_6 shows similar results but specific electronic structure calculations exploring the FS are required to elucidate the mechanism and the effect of the magnetic field.

It is worth mentioning that Fig. 4 suggests the absence of magnetic impurities in our samples that produce a diamagnetic response. At $T \geqslant 100$ K, the system exhibits ac frequency-independent diamagnetic character associated with a good metal. Below 100 K, YCd_6 presents frequency and temperature dependencies of the diamagnetic response, which is an anomalous observation [32] since frequency dependence is understood as resulting from glassiness or progressive spin freezing, and therefore would not at all be expected for diamagnetic systems.

Although the frequency-dependent data below 100 K in χ' and χ'' reveal unusual features, one of the possible explanations of this anomalous behavior is the skin depth effect in a metal that could account for the observed anomalies. According to this idea, it is expected that χ' becomes negligible at the maximum skin depth and the corresponding χ'' becomes maximum. In the case of YCd_6, Figs. 4(a) and 4(b) suggest that both quantities χ' and χ'' maximize at the same frequency. With this we can rule out this hypothesis. Another point of view is to consider the existence of magnetic domains with different sizes. The emergence of diamagnetic domains (Condon domains) relates to the observation of de Haas–van Alphen (dHvA) oscillations [33] as was the case of beryllium and silver. In both cases the dHvA amplitude was comparable with the oscillation period developing Condon domains explicitly. However, as depicted in Figs. 5 and 6, there is no clear evidence of well-defined oscillations. Hence, it is possible that the dHvA amplitude (as in most metals) is significantly smaller than the oscillation period even in high-quality single crystals at very low temperatures. With this, we can ignore the existence of diamagnetic domains. Since the imaginary part of the ac susceptibility is correlated with dissipative effects in the sample, the frequency-dependent data below 100 K observed in Figs. 4(a) and 4(b) suggest a strong magnetic dynamic behavior despite the lack of magnetic order. This behavior is observed in unconventional superconductors of magnetic origin [34] and in quantum magnets [35]. However, the magnetic response of a metal to an external magnetic field in a quantum-mechanical scenario of the metal's bulk properties forbids any temperature and frequency dependence of the diamagnetic behavior under ac magnetic field. These results are in agreement with the observations in ac measurements

for the metal NiSi [32] where its origin is not yet understood. The ac susceptibility similarities between NiSi and YCd_6 are remarkable and warrant further theoretical and experimental investigations to reveal a closer perspective to the underlying mechanism.

IV. CONCLUSIONS

Our experimental results show giant magnetoresistance in YCd_6 at low temperatures and high magnetic fields. MR has a field dependence evolution of $\rho/\rho(0)$: $\sim\mu_0 H^2$ above 50 K, $\sim\mu_0 H^1$ (from 25 to 50 K), and $\sim\mu_0 H^{0.5}$ (from 0.4 to 5.65 K) in transverse TMR experiments together with a continuous evolution from $\mu_0 H^{0.8}$ to $\mu_0 H^{0.3}$ in LMR experiments. When compared with elemental metals as Ag and Cu, LMR experiments in YCd_6 shows a similar saturation up to high fields suggesting a complex FS. These results indicate strong anisotropy in the band structure and a magnetic field dependence of the FS topology.

The observed magnetoresistive effect could be explained considering different T-dependent mobilities for different electronic bands. The field dependence with exponent smaller than 1.0 can be understood as resulting in electron and hole bands having different carrier densities, or a lack of compensation, and different mobilities. Exploring MR in this QCA system is a fundamental task in understanding the electronic structure, Fermi surfaces, and general electronic properties of periodic systems providing the basis for the interpretation of electronic properties in more complex systems as QCs.

ACKNOWLEDGMENTS

The work at UFPE was supported by Brazilian agencies FACEPE, CNPq, FINEP, and CAPES. The National High Magnetic Field Laboratory is supported by the National Science Foundation through NSF/DMR-1644779 and the State of Florida. L.B. is supported by the U.S.-DOE through the BES program Award No. DE-SC0002613.

[1] M. N. Baibich, J. M. Broto, A. Fert, F. Nguyen Van Dau, F. Petroff, P. Etienne, G. Creuzet, A. Friederich, and J. Chazelas, Phys. Rev. Lett. **61**, 2472 (1988).
[2] R. B. van Dover, E. M. Gyorgy, R. J. Cava, J. J. Krajewski, R. J. Felder, and W. F. Peck, Phys. Rev. B **47**, 6134 (1993).
[3] L. Morellon, P. A. Algarabel, C. Magen, and M. R. Ibarra, J. Magn. Magn. Mater. **237**, 119 (2001).
[4] J. Sakurai, S. Nakatani, A. Adam, and H. Fujiwara, J. Magn. Magn. Mater. **108**, 143 (1992).
[5] R. Jha, S. Onishi, R. Higashinaka, T. D. Matsuda, R. A. Ribeiro, and Y. Aoki, AIP Adv. **8**, 101332 (2018).
[6] S. Thirupathaiah, R. Jha, B. Pal, J. S. Matias, P. K. Das, P. K. Sivakumar, I. Vobornik, N. C. Plumb, M. Shi, R. A. Ribeiro, and D. D. Sarma, Phys. Rev. B **95**, 241105(R) (2017).
[7] A. Pariari, R. Singha, S. Roy, B. Satpati, and P. Mandal, Sci. Rep. **8**, 10527 (2018).
[8] P. Kumar, Sudesh, and S. Patnaik, J. Phys. Commun. **3**, 115007 (2019).
[9] H. Takatsu, J. J. Ishikawa, S. Yonezawa, H. Yoshino, T. Shishidou, T. Oguchi, K. Murata, and Y. Maeno, Phys. Rev. Lett. **111**, 056601 (2013).
[10] E. Mun, H. Ko, G. J. Miller, G. D. Samolyuk, S. L. Bud'ko, and P. C. Canfield, Phys. Rev. B **85**, 035135 (2012).
[11] S. N. Zhang, Q. S. Wu, Y. Liu, and O. V. Yazyev, Phys. Rev. B **99**, 035142 (2019).
[12] A. I. Goldman, T. Kong, A. Kreyssig, A. Jesche, M. Ramazanoglu, K. W. Dennis, S. L. Bud'ko, and P. C. Canfield, Nat. Mater. **12**, 714 (2013).
[13] T. Kong, S. L. Bud'ko, A. Jesche, J. McArthur, A. Kreyssig, A. I. Goldman, and P. C. Canfield, Phys. Rev. B **90**, 014424 (2014).
[14] A. Mori, H. Ota, S. Yoshiuchi, K. Iwakawa, Y. Taga, Y. Hirose, T. Takeuchi, E. Yamamoto, Y. Haga, F. Honda *et al.*, J. Phys. Soc. Jpn. **81**, 024720 (2012).
[15] M. Cabrera-Baez, M. A. Avila, and C. Rettori, Phys. Rev. B **100**, 014207 (2019).
[16] Y. Ishii and T. Fujiwara, J. Alloys Compd. **342**, 343 (2002).
[17] P. C. Canfield and Z. Fisk, Philos. Mag. B **65**, 1117 (1992).
[18] S. K. Dhar, A. Palenzona, P. Manfrinetti, and S. M. Pattalwar, J. Phys.: Condens. Matter **14**, 517 (2002).
[19] C. P. Gómez and S. Lidin, Phys. Rev. B **68**, 024203 (2003).
[20] A. B. Pippard, *Magnetoresistance in Metals* (Cambridge University Press, Cambridge, UK, 2009).
[21] J. M. D. Coey, *Magnetism and Magnetic Materials* (Cambridge University Press, Cambridge, UK, 2009).
[22] J. M. Ziman, *Electrons and Phonons: The Theory of Transport Phenomena in Solids* (Oxford University Press, Oxford, UK, 2001).
[23] N. Nandi, T. Scaffidi, P. Kushwaha, S. Khim, M. E. Barber, V. Sunko, F. Mazzola, P. D. C. King, H. Rosner, P. J. W. Moll *et al.*, npj Quantum Mater. **3**, 66 (2018).
[24] B. N. Narozhny, Riv. Nuovo Cimento **45**, 661 (2022).
[25] G. Varnavides, Y. Wang, P. J. W. Moll, P. Anikeeva, and P. Narang, Phys. Rev. Mater. **6**, 045002 (2022).
[26] B. Lüthi, Phys. Rev. Lett. **2**, 503 (1959).
[27] J. O. Strom-Olsen, Proc. R. Soc. Lond. A **302**, 83 (1967).
[28] H. K. Pal and D. L. Maslov, Phys. Rev. B **81**, 214438 (2010).
[29] A. B. Pippard, Proc. R. Soc. Lond. A **282**, 464 (1964).
[30] K. Wang, D. Graf, L. Li, L. Wang, and C. Petrovic, Sci. Rep. **4**, 7328 (2014).
[31] A. N. Perevalova, S. V. Naumov, S. M. Podgornykh, E. B. Marchenkova, V. V. Chistyakov, J. C. A. Huang, and V. V. Marchenkov, AIP Adv. **12**, 035225 (2022).
[32] A. Dahal, J. Gunasekera, L. Harriger, S. H. Lee, Y. S. Hor, D. J. Singh, and D. K. Singh, Phys. Rev. B **94**, 184516 (2016).
[33] V. S. Egorov, Phys. Usp. **53**, 755 (2010).
[34] S. H. Lee, H. Kikuchi, Y. Qiu, B. Lake, Q. Huang, K. Habicht, and K. Kiefer, Nat. Mater. **6**, 853 (2007).
[35] J. M. Tranquada, H. Woo, T. G. Perring, H. Goka, G. D. Gu, G. Xu, M. Fujita, and K. Yamada, Nature (London) **429**, 534 (2004).